



Full paper/Mémoire

Star-shaped Keggin-type heteropolytungstate nanostructure as a new catalyst for the preparation of quinoxaline derivatives

Majid Masteri-Farahani^{a,*}, Melika Ghorbani^a, Ali Ezabadi^b, Niki Farrokhinia^b, Atekeh-Sadat Ghaemmaghami^b

^a Faculty of Chemistry, Kharazmi University, Tehran, Iran

^b Department of Chemistry, Central Tehran Branch, Islamic Azad University, Tehran, Iran

ARTICLE INFO

Article history:

Received 18 October 2013

Accepted after revision 28 January 2014

Available online 16 September 2014

Keywords:

Heteropolytungstate

Keggin

Nanostructure

Microemulsion

Quinoxaline

Catalyst

ABSTRACT

In this work, we report the novel successful preparation of the Keggin-type Cs(CTA)₂PW₁₂O₄₀ (CTA = cetyltrimethylammonium cation) nanostructure by a microemulsion method. The microemulsion system included the cationic surfactant CTAB, 1-butanol as co-surfactant, isooctane as oil phase, and an aqueous solution containing CsNO₃. The Cs(CTA)₂PW₁₂O₄₀ nanostructure was formed by the addition of an aqueous solution of phosphotungstic acid to the microemulsion solution. Characterization of the resultant nanostructure was done using FT-IR spectroscopy, X-ray diffraction, scanning electron microscopy, energy-dispersive X-ray analysis, and CHN elemental analysis. The product was found to be a star-shaped nanostructure composed of some nanorods whose diameter and length are about 100 nm and 500 nm, respectively. The prepared nanostructure was used as a recoverable catalyst for the synthesis of quinoxaline derivatives by the condensation of 1,2-diamines with 1,2-dicarbonyl compounds, which afforded the products in good to high yields in short reaction times.

© 2014 Académie des sciences. Published by Elsevier Masson SAS. All rights reserved.

1. Introduction

The synthesis of quinoxaline and of its derivatives played an important role in organic synthesis because of their wide range of biological activities, such as anti-bacterial [1], antidepressant [2], anti-inflammatory [3], and antitumor [4] ones. Due to their great importance, many synthetic strategies have been developed for the synthesis of quinoxalines [5–9]. However, most of these methodologies involve pollution, long reaction time and difficult work-up and recovery of the catalysts, leaving considerable scope for the development of further clean, facile and efficient catalytic processes for these important molecules. Condensation of a 1,2-diamine with a 1,2-dicarbonyl compound in the presence of Brønsted or Lewis

acids, such as montmorillonite K-10 [10], mesoporous silica SBA-15 covalently anchored with copper (II) Schiff base complex [11], alumina [12], and silica-supported perchloric acid [13], Wells–Dawson heteropoly acid (H₆P₂W₁₈O₆₂·24H₂O) [14], iron exchanged molybdophosphoric acid [15], and Keggin-type H₄SiW₁₂O₄₀ heteropoly acid [16], is one of the important methods for the preparation of quinoxalines. However, to the best of our knowledge, there is no any example of the use of nanostructured Keggin-type heteropolyanions as catalysts for the synthesis of quinoxaline derivatives.

Heteropoly acids are discrete metal–oxygen clusters built from the connection of MO_x polyhedra in which M is a d-block element in a high oxidation state [17–20]. They possess both acidic and redox properties and thus are of great importance for practical applications, especially in catalysis [21–28]. Pure heteropoly acids have high solubility in polar reaction systems, which hinders their applications as heterogeneous catalysts and so results in

* Corresponding author.

E-mail address: mfarahany@yahoo.com (M. Masteri-Farahani).

separation problems during the isolation of the product after completion of the reaction. It has been found that water-insoluble salts of heteropoly acids with large cations, such as Cs^+ , K^+ , NH_4^+ , and organic cations can be used as efficient heterogeneous catalysts [28–30]. These compounds are prepared by partial or complete cation exchange with protons in heteropoly acids. For example, a caesium salt of $\text{H}_3\text{PW}_{12}\text{O}_{40}$, $\text{Cs}_{2.5}\text{H}_{0.5}\text{PW}_{12}\text{O}_{40}$ has lately gained attention because of strong acidity and insolubility in water and organic solvents, and so can be considered as a solid acid catalyst. This salt was reported to exhibit significantly higher activity than the parent acid in gas-phase acid-catalyzed reactions [28–31].

Polyoxometalate nanostructures have attracted considerable interest owing to their interesting properties and wide range of applications [32–36]. Some methods have been developed for the preparation of polyoxometalate nanostructures, such as homogeneous precipitation using decomposition of urea [35], solid-state chemical reaction [36], and microemulsion methods [37,38].

Recently, we have reported the first successful one-pot preparation and characterization of heteropolymolybdate nanoparticles with a microemulsion method [38]. Microemulsions are systems composed of a mixture of an aqueous phase, an oil phase, a surfactant, and a co-surfactant [39–41]. They are transparent solutions that are thermodynamically stable and optically isotropic. The nanosized water droplets in microemulsions act as nanoreactors for producing the desired nanostructures. The advantage of this method is the good control on the size and morphology of the prepared nanostructure.

Here, we further explore the potential of microemulsion method for the preparation of a novel $\text{Cs}(\text{CTA})_2\text{PW}_{12}\text{O}_{40}$ nanostructure. The prepared nanostructure acts as a recoverable heterogeneous catalyst for green and efficient synthesis of quinoxaline derivatives in high yields and short reaction times. In comparison with previous catalytic systems for the synthesis of quinoxaline derivatives [10–16], it has the following advantages: easy recoverability, comparable yields with short reaction times, and especially solvent-free conditions that make it an environmentally friendly and cost-effective process.

2. Experimental

2.1. Materials and instrumentations

All chemicals were purchased from Merck Chemicals and used without further purification. Phosphotungstic acid was prepared by a method taken from the literature [28].

FT-IR spectra were recorded with a PerkinElmer Spectrum RXI FT-IR spectrometer using pellets of the materials diluted with KBr. X-ray powder diffraction measurements (XRD) were performed on a SIEFERT XRD 3003 PTS diffractometer using $\text{Cu K}\alpha$ radiation (wavelength $\lambda = 0.154$ nm). The patterns were recorded from 5° to 80° with steps of 0.02° every second. Scanning electron microscopy images were taken with a ZEISS-DSM 960A microscope with an attached camera operating at 30 kV.

DR UV-Vis spectra were collected using a PG Instrument Ltd T90+ UV-Vis Spectrometer with BaSO_4 as a standard. Elemental analyses were performed using a scanning electron microscope equipped with EDX detector INCA Penta FETx3. 1. The carbon and nitrogen contents of the samples were analyzed using a Thermo Finnigan (Flash 1112 Series EA) CHN Analyzer. ^1H NMR spectra were recorded on a Bruker AQS AVANCE-300 MHz spectrometer using TMS as an internal standard. All products were well characterized by comparison with authentic samples by TLC, spectral and physical data recording.

2.2. Preparation of the $\text{Cs}(\text{CTA})_2\text{PW}_{12}\text{O}_{40}$ nanostructure

The quaternary microemulsion system consisted of $\text{H}_2\text{O}/\text{CTAB}/\text{isooctane}/n\text{-butanol}$ and had been prepared as follows: CTAB (2 g) in water (2 mL) was added to a stirred solution of n -butanol (2 g) and isooctane (4 g). Then, 1 mL CsNO_3 (0.5 M) in water was added to the above mixture and stirred for 10 min to give a transparent solution. Under stirring, 1 mL of $\text{H}_3\text{PW}_{12}\text{O}_{40}$ (0.5 M) was added and the reaction continued for another 2 h. The resultant white product was collected by centrifugation and washed several times with water and ethanol to remove the remaining organic residue and dried at 110°C for 12 h.

2.3. General method for the preparation of quinoxaline derivatives

A mixture of 1,2-dicarbonyl (1 mmol) and 1,2-diamine (1 mmol) derivatives in the presence of an appropriate amount of the $\text{Cs}(\text{CTA})_2\text{PW}_{12}\text{O}_{40}$ catalyst was stirred at a given temperature. The progress of the reaction was monitored by thin layer chromatography (TLC). After completion of the reaction, 5 mL of hot ethanol was added to the reaction mixture and the solid catalyst was filtered. The pure products were obtained after crystallization and analyzed without any further purification. All of the obtained quinoxalines are known compounds and identified by ^1H NMR and melting points compared with the literature values. The melting points, spectral (^1H NMR) and elemental analysis data for the products are given below.

2.4. 2,3-Diphenyl-quinoxaline

Mp. $120\text{--}122^\circ\text{C}$; ^1H NMR (500 MHz, CDCl_3): δ (ppm): 8.20 (d, d, 3.35, 3.35 Hz, 2H), 7.79 (dd, 3.3, 3.35 Hz, 2H), 7.54 (d, $J = 6.65$ Hz, 4H), 7.38 (m, 6H); FT-IR (KBr): 3059, 1436, 1395, 1341, 707, 695 cm^{-1} . Anal. calcd. for $\text{C}_{20}\text{H}_{14}\text{N}_2$: C, 85.08; H, 5.00; N, 9.92. Found: C, 85.25; H, 5.12; N, 9.98.

2.5. 2,3-Bis(4-methoxyphenyl) quinoxaline

Mp. $140\text{--}141^\circ\text{C}$; ^1H NMR (500 MHz, CDCl_3): δ (ppm): 8.14 (m, 2H), 7.73 (m, 2H), 7.51 (d, $J = 8.25$ Hz, 4H), 6.89 (d, $J = 8.25$ Hz, 4H), 3.85 (s, 6H); FT-IR (KBr): 2936, 2836, 1603, 1509, 1340, 1293, 1245, 832 cm^{-1} . Anal. calcd. for $\text{C}_{22}\text{H}_{18}\text{N}_2\text{O}_2$: C, 77.17; H, 5.30; N, 8.18. Found: C, 76.97; H, 5.21; N, 8.01.

2.6. 2,3-Di-p-tolyl quinoxaline

Mp. 147–148 °C; $^1\text{H NMR}$ (500 MHz, CDCl_3): δ (ppm): 8.17 (m, 2H), 7.75 (m, 2H), 7.44 (d, $J = 7.75$ Hz, 4H), 7.16 (d, $J = 7.65$ Hz, 4H), 2.38 (s, 6H); FT-IR (KBr): 2911, 1610, 1462, 1396, 1337, 1210, 758 cm^{-1} . Anal. calcd. for $\text{C}_{22}\text{H}_{18}\text{N}_2$: C, 85.13; H, 5.84; N, 9.03. Found: C, 84.91; H, 5.71; N, 8.89.

2.7. 2,3-Di (furan-2-yl) quinoxaline

Mp. 128–130 °C; $^1\text{H NMR}$ (500 MHz, CDCl_3): δ (ppm): 8.18 (dd, $J = 3.4$ Hz, 2H), 7.78 (dd, $J = 3.25$ Hz, 2H), 7.65 (s, 2H), 6.71 (s, 2H), 6.59 (s, 2H); FT-IR (KBr): 3107, 1566, 1485, 1397, 1328, 755 cm^{-1} . Anal. calcd. for $\text{C}_{16}\text{H}_{10}\text{N}_2\text{O}_2$: C, 73.27; H, 3.84; N, 10.68. Found: C, 73.48; H, 3.96; N, 10.77.

2.8. 6-Methyl-2,3-diphenyl quinoxaline

Mp. 109–110 °C; $^1\text{H NMR}$ (500 MHz, CDCl_3): δ (ppm): 8.08 (d, $J = 8.45$ Hz, 1H), 7.97 (s, 1H), 7.63 (d, $J = 8.3$ Hz, 1H), 7.52 (d, $J = 6.3$ Hz, 4H), 7.35 (d, $J = 6.9$ Hz, 6H), 2.62 (s, 3H); FT-IR (KBr): 3050, 1615, 1482, 1441, 1340, 697 cm^{-1} . Anal. calcd. for $\text{C}_{21}\text{H}_{16}\text{N}_2$: C, 85.11; H, 5.44; N, 9.45. Found: C, 85.24; H, 5.56; N, 9.52.

2.9. 2,3-Bis (4-methoxyphenyl)-6-methylquinoxaline

Mp. 120–121 °C; $^1\text{H NMR}$ (500 MHz, CDCl_3): δ (ppm): 8.03 (d, $J = 8.45$ Hz, 1H), 7.92 (s, 1H), 7.57 (d, $J = 8.25$ Hz, 1H), 7.49 (d, $J = 6.5$ Hz, 4H), 6.88 (d, $J = 8.25$ Hz, 4H), 3.84 (s, 6H), 2.61 (s, 3H); FT-IR (KBr): 2925, 1599, 1259, 833 cm^{-1} . Anal. calcd. for $\text{C}_{23}\text{H}_{20}\text{N}_2\text{O}_2$: C, 77.51; H, 5.66; N, 7.86. Found: C, 77.63; H, 5.75; N, 7.96.

2.10. 6-Methyl-2,3-di-p-tolyl quinoxaline

Mp. 135–136 °C; $^1\text{H NMR}$ (500 MHz, CDCl_3): δ (ppm): 8.05 (d, $J = 8.4$ Hz, 1H), 7.94 (s, 1H), 7.59 (d, $J = 8.2$ Hz, 1H), 7.43 (d, $J = 6.8$ Hz, 4H), 7.15 (d, $J = 7.4$ Hz, 4H), 2.61 (s, 3H), 2.38 (s, 6H); FT-IR (KBr): 3036, 2917, 1613, 1445, 1340, 824 cm^{-1} . Anal. calcd. for $\text{C}_{23}\text{H}_{20}\text{N}_2$: C, 85.15; H, 6.21; N, 8.63. Found: C, 85.05; H, 6.12; N, 8.51.

2.11. 2,3-Di (furan-2-yl)-6-methyl quinoxaline

Mp. 113–114 °C; $^1\text{H NMR}$ (500 MHz, CDCl_3): δ (ppm): 8.13 (d, $J = 8.3$ Hz, 1H), 8.057 (s, 1H), 7.64 (m, 3H), 6.77 (d, $J = 18.75$ Hz, 2H), 6.60 (s, 2H), 2.62 (s, 3H); FT-IR (KBr): 3110, 2917, 1615, 1563, 1491, 1329, 752 cm^{-1} . Anal. calcd. for $\text{C}_{17}\text{H}_{12}\text{N}_2\text{O}_2$: C, 73.90; H, 4.38; N, 10.14. Found: C, 74.01; H, 4.45; N, 10.21.

2.12. 2,3-Dimethyl quinoxaline

Mp. 104–106 °C; $^1\text{H NMR}$ (500 MHz, CDCl_3): δ (ppm): 7.97 (m, 2H), 7.65 (m, 2H), 2.72 (s, 6H) ppm; FT-IR (KBr): 3020, 2930, 1648, 1485, 760 cm^{-1} . Anal. calcd. for $\text{C}_{10}\text{H}_{10}\text{N}_2$: C, 75.92; H, 6.37; N, 17.71. Found: C, 75.85; H, 6.26; N, 17.62.

2.13. 5,6-Diphenyl-2,3-dihydro pyrazine

Mp. 160–161 °C; $^1\text{H NMR}$ (500 MHz, CDCl_3): δ (ppm): 7.41 (d, $J = 7.4$ Hz, 6H), 7.33 (d, $J = 6.6$ Hz, 4H), 3.73 (s, 4H); FT-IR (KBr): 3040, 2946, 1549, 1437, 984, 694 cm^{-1} . Anal. calcd. for $\text{C}_{16}\text{H}_{14}\text{N}_2$: C, 82.02; H, 6.02; N, 11.96. Found: C, 82.12; H, 6.10; N, 12.01.

2.14. 5,6-Di-p-tolyl-2,3-dihydro pyrazine

Mp. 164–166 °C; $^1\text{H NMR}$ (500 MHz, CDCl_3): δ (ppm): 7.31 (d, $J = 8.15$ Hz, 4H), 7.06 (d, $J = 7.85$ Hz, 4H), 3.67 (s, 4H), 2.32 (s, 6H); FT-IR (KBr): 3029, 2959, 1611, 1552, 982, 822 cm^{-1} . Anal. calcd. for $\text{C}_{18}\text{H}_{18}\text{N}_2$: C, 82.41; H, 6.92; N, 10.68. Found: C, 82.49; H, 7.02; N, 10.77.

3. Results and discussion

3.1. Preparation of $\text{Cs}(\text{CTA})_2\text{PW}_{12}\text{O}_{40}$ nanostructure

The $\text{Cs}(\text{CTA})_2\text{PW}_{12}\text{O}_{40}$ nanostructure was prepared by partial exchange of the protons of phosphotungstic acid by caesium ions in the nanoreactors of the water droplets in the microemulsion system. The sequence of events was shown in Fig. 1. Stoichiometric addition of phosphotungstic acid solution to the caesium-containing microemulsion system results in the formation of a $\text{Cs}(\text{CTA})_2\text{PW}_{12}\text{O}_{40}$ nanostructure, which is insoluble in water and organic solvents and precipitates immediately. On the other hand, the CTAB species act as protecting groups against the assembly and growth of the as-prepared nanostructure.

3.2. Spectroscopic characterization of the $\text{Cs}(\text{CTA})_2\text{PW}_{12}\text{O}_{40}$ nanostructure

FT-IR spectroscopy was used to check whether the Keggin structure is preserved in the prepared nanostructure. In the FT-IR spectrum of the $\text{Cs}(\text{CTA})_2\text{PW}_{12}\text{O}_{40}$ nanostructure (Fig. 2), the four main features of the

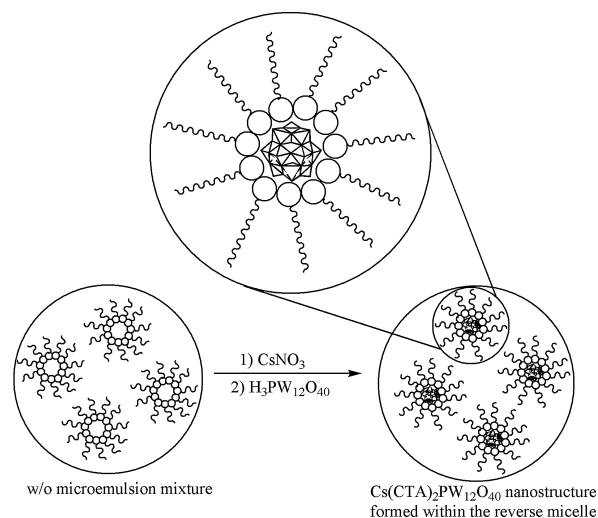


Fig. 1. Schematic illustration for the preparation of the $\text{Cs}(\text{CTA})_2\text{PW}_{12}\text{O}_{40}$ nanostructure.

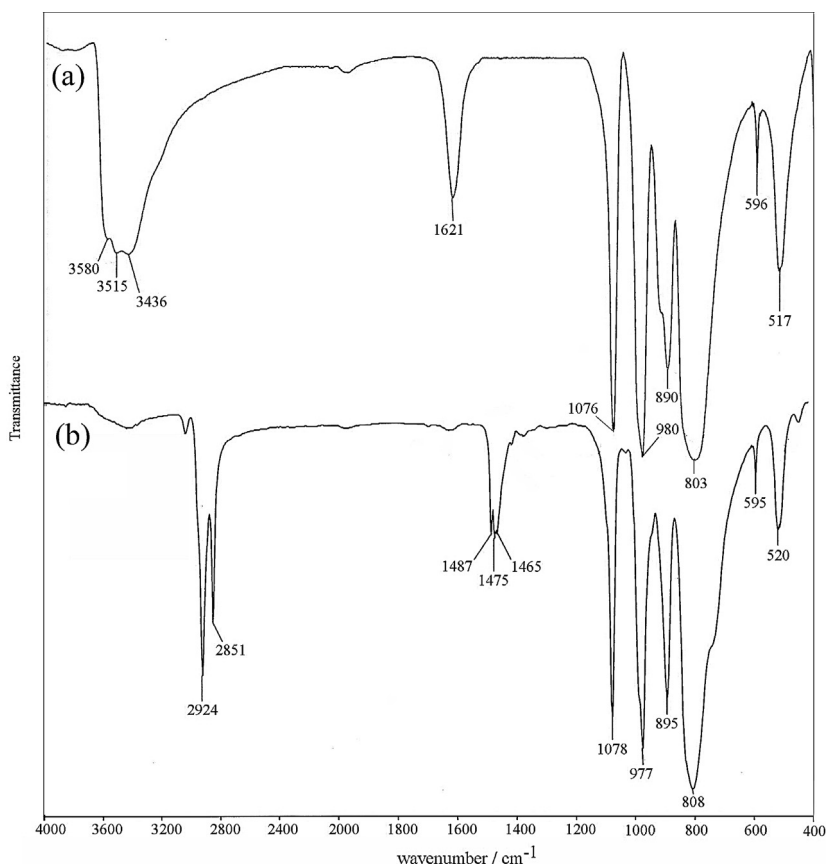


Fig. 2. FT-IR spectra of (a) $\text{H}_3\text{PW}_{12}\text{O}_{40}$, and (b) $\text{Cs}(\text{CTA})_2\text{PW}_{12}\text{O}_{40}$ nanostructures.

Keggin-type phosphotungstate anions [42] for the prepared nanostructure are observed at 1078 cm^{-1} ($\nu_{\text{as, p-o}}$), 977 cm^{-1} ($\nu_{\text{as, wo}}$), 895 cm^{-1} ($\nu_{\text{as, corner, sharing W-O-W}}$) and 808 cm^{-1} ($\nu_{\text{as, edge sharing W-O-W}}$). Compared with bulk $\text{H}_3\text{PW}_{12}\text{O}_{40}$, the observed blue shift of $\nu_{\text{as, corner sharing W-O-W}}$ and $\nu_{\text{as, edge sharing W-O-W}}$ peaks in $\text{Cs}(\text{CTA})_2\text{PW}_{12}\text{O}_{40}$ nanostructures results from the substitution of the H^+ by Cs^+ and CTA^+ cations with stronger interactions, since it has been shown that the protons in the heteropoly acids are linked to the bridging oxygens rather than to terminal oxygens. On the other hand, the bands at 2851 and 2924 cm^{-1} are attributed to the symmetric and asymmetric C-H stretching vibrations of the CH_2 groups of CTAB species associated with the $\text{Cs}(\text{CTA})_2\text{PW}_{12}\text{O}_{40}$ nanostructure. Also, the bands at $1400\text{--}1500\text{ cm}^{-1}$ were assigned to the symmetric and asymmetric C-H deformations. A noteworthy feature in this spectrum is the significant absence of O-H stretching vibrations near $3400\text{--}3700\text{ cm}^{-1}$, which indicates the hydrophobic and water tolerant nature of the prepared nanostructure. Thus, the FT-IR spectrum of the product showed the existence of the Keggin-type nanostructure associated with CTAB species.

The UV-Vis spectrum of the $\text{Cs}(\text{CTA})_2\text{PW}_{12}\text{O}_{40}$ nanostructure is presented in Fig. 3. In the UV-Vis spectra of Keggin heteropolyanions, there are two main absorptions corresponding to the ligand-to-metal charge transfer (from mainly oxygen 2p orbitals to mainly metal d orbitals) [43]. In

the represented spectrum, the strong peak at 265 nm is assigned to an oxygen-to-tungsten charge transfer in edge-shared WO_6 octahedra and the shoulder at 330 nm is attributed to an oxygen-to-tungsten charge transfer in corner-shared WO_6 octahedra, which further confirms the presence of a Keggin-type $\text{Cs}(\text{CTA})_2\text{PW}_{12}\text{O}_{40}$ nanostructure.

3.3. X-ray analyses of the $\text{Cs}(\text{CTA})_2\text{PW}_{12}\text{O}_{40}$ nanostructure

The X-ray diffraction pattern of $\text{Cs}(\text{CTA})_2\text{PW}_{12}\text{O}_{40}$ nanostructure is shown in Fig. 4a. As can be seen in the

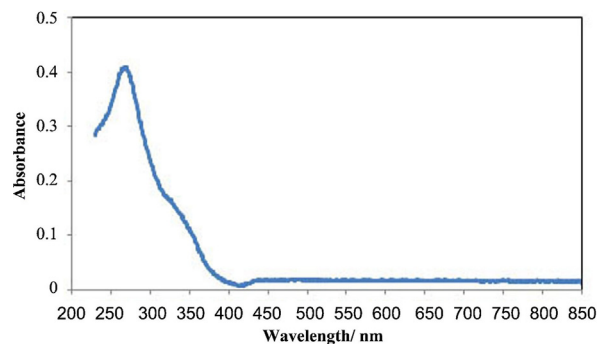


Fig. 3. (Color online.) UV-Vis spectrum of the $\text{Cs}(\text{CTA})_2\text{PW}_{12}\text{O}_{40}$ nanostructure.

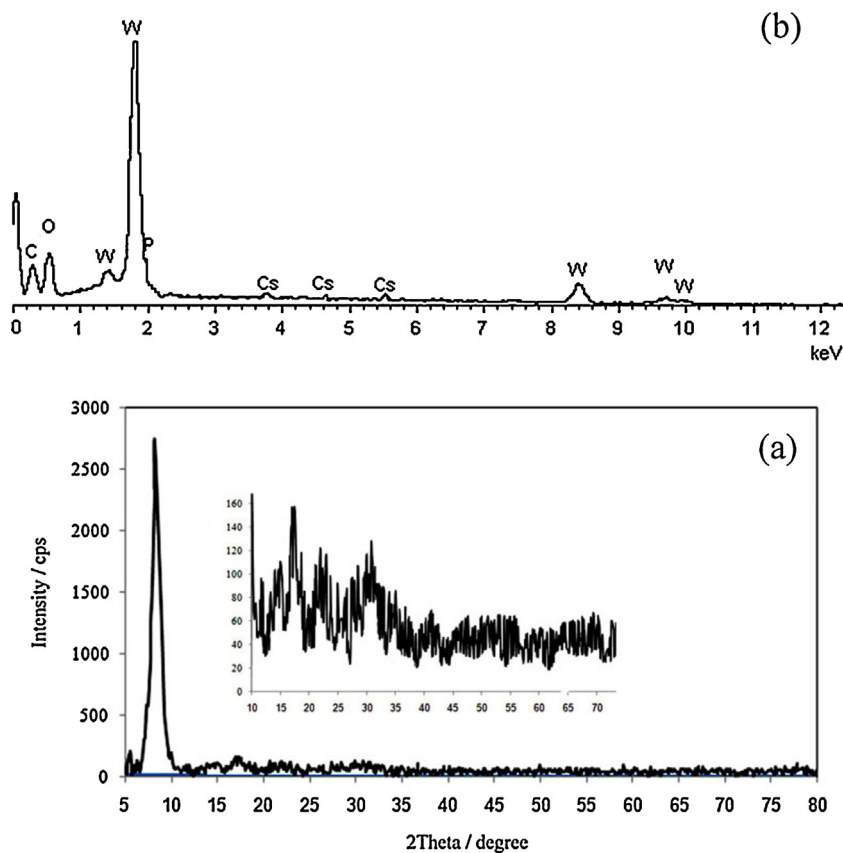


Fig. 4. (a) X-ray diffraction pattern and (b) energy-dispersive X-ray analysis of the $\text{Cs}(\text{CTA})_2\text{PW}_{12}\text{O}_{40}$ nanostructure.

XRD pattern of the $\text{Cs}(\text{CTA})\text{PW}_{12}\text{O}_{40}$ nanostructure, only one intense peak at about $2\theta = 8^\circ$ is observable, which is a typical feature of the Keggin structure [28]; the other peaks are very weak and broad. These observations indicate that, unlike the parent phosphotungstic acid, the prepared nanostructure has no good crystalline nature and is mainly amorphous. The long-chain hexadecyl groups in the prepared nanostructure inhibit the good ordering of the individual Keggin units to form any crystalline phase. Moreover, this can be also a result of the small size of the prepared nanostructure and of the absence of any crystal plane.

Stoichiometry and chemical composition of the prepared nanomaterial was examined by energy-dispersive X-ray analysis (EDX) and CHN analysis. EDX analysis of the nanocrystals in Fig. 4b showed the molar ratio Cs:P:W of 1.1:1:11.7. On the other hand, CHN analysis showed 12.89% of carbon and 0.82% of nitrogen, which showed the presence of 2 equiv of CTA^+ cations in the product. These values are close to the stoichiometric composition and further confirm the formation of the $\text{Cs}(\text{CTA})_2\text{PW}_{12}\text{O}_{40}$ nanostructure.

3.4. Scanning electron microscopy analysis and formation mechanism of the prepared nanostructure

The morphology and microstructure of the $\text{Cs}(\text{CTA})_2\text{PW}_{12}\text{O}_{40}$ nanostructure were investigated with

scanning electron microscopy. A typical SEM image of the obtained nanoparticles after 5 min is shown in Fig. 5a. As can be seen in this figure, the product is composed of nearly spherical particles. With stoichiometric addition of phosphotungstic acid solution to the caesium-containing microemulsion system, the nucleation of the nanostructure occurs immediately in the nanoreactors of the water droplets, and nanoparticles with surfactant coatings are formed in a very short time. But with collision of the reverse micelles, the coalescence of the nearly spherical nanoparticles shows the morphological evolution of a new nanostructure as a function of the processing time. When processed for 2 h, the aggregation between the spherical nanoparticles was induced by the coalescence process, resulting in the agglomeration and growth of star-shaped nanostructures. Fig. 5b shows that each nanostructure is composed of some nanorods whose diameter and length are about 100 nm and 500 nm, respectively, and extending radially from the centre.

3.5. Investigation of the catalytic activity of the $\text{Cs}(\text{CTA})_2\text{PW}_{12}\text{O}_{40}$ nanostructure in the preparation of quinoxaline derivatives

The catalytic properties of the $\text{Cs}(\text{CTA})_2\text{PW}_{12}\text{O}_{40}$ nanostructure were examined in the preparation of quinoxaline derivatives. The prepared nanostructure can activate the carbonyl compounds and facilitate the attack

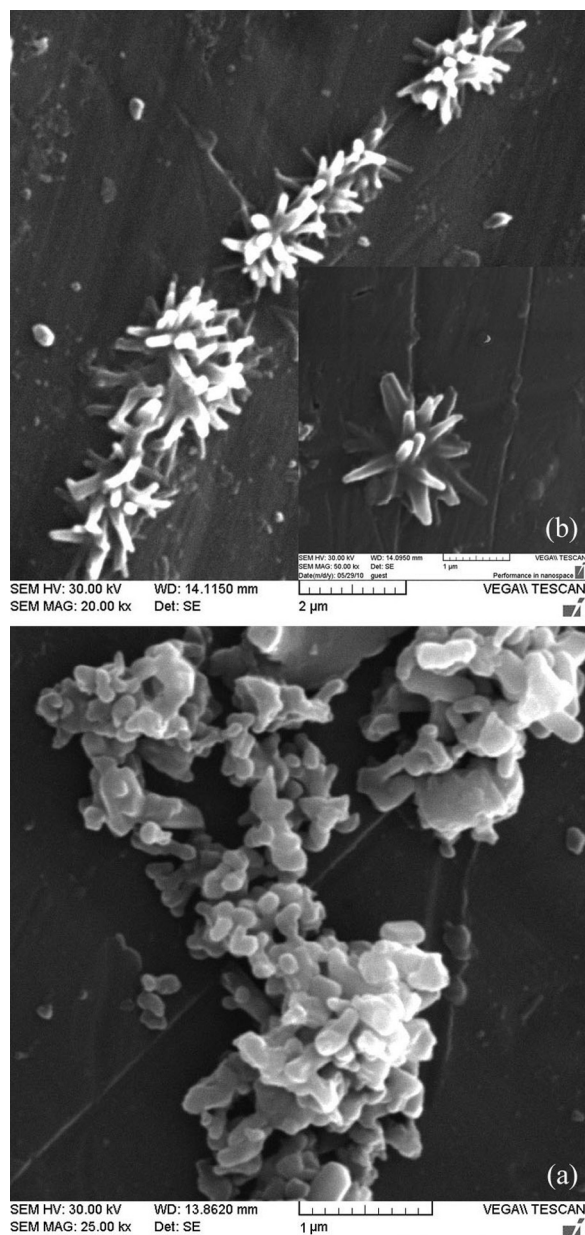


Fig. 5. Scanning electron microscopy images of (a) the obtained nanoparticles after 5-min stirring of the reaction mixture, and (b) the final $\text{Cs}(\text{CTA})_2\text{PW}_{12}\text{O}_{40}$ nanostructure.

of the amino groups to carbonyl compounds. The reaction proceeded in a one-pot procedure and free of side products.

In order to find the optimum conditions for the synthesis of quinoxalines derivatives, we investigated the effect of solvent, temperature and catalyst amounts on the model reaction between benzil and *o*-phenylenediamine.

Table 1 presents the results of condensation reactions in various solvents, including CH_2Cl_2 , CH_3CN , H_2O , $\text{C}_2\text{H}_5\text{OH}$, and $\text{CH}_3\text{COOC}_2\text{H}_5$. The results of performing the reaction in solvent-free conditions as well as the effect of the

Table 1
Effect of various solvents on the synthesis of quinoxaline.

Entry	Solvent	Time (h)	Yield (%)
1	Ethanol	4:00	77
3	Water	6:00	40
4	Dichloromethane	11:00	90
5	Acetonitrile	15:00	91
6	Ethyl acetate	13:00	72

Reaction conditions: benzil (1.0 mmol), *o*-phenylenediamine (1.0 mmol), catalyst (25 mg), solvent (5 mL), reflux conditions.

temperature on the reaction times and yields have been shown in Table 2. It can be seen that the increase of reaction temperature led to the enhancement of the yield of quinoxaline. On the other hand, in the absence of the catalyst the reaction did not complete even after 24 h.

Since the recyclability of the catalyst is crucial to its application, we conducted an experiment to evaluate the recyclability of the $\text{Cs}(\text{CTA})_2\text{PW}_{12}\text{O}_{40}$ nanostructure in the catalytic preparation of quinoxaline derivatives. After filtration, the catalyst was washed several times with ethanol and dried in a vacuum oven. Then, it was used in the reaction with a fresh reaction mixture and the result is given in Table 2. As can be seen, the product yield showed no significant decrease, implying that the nanostructure was stable and retained its activity during the catalytic cycle. On the other hand, the FT-IR spectrum of the recycled catalyst (not shown here) showed the characteristic bands of the original catalyst, indicating the stability of the catalyst during the course of the catalytic reaction.

In order to show the generality of this method, we used some substituted 1,2-phenylenediamines and diketones under optimized conditions in solvent-free conditions, and the results are summarized in Table 3. All the reactions proceeded very cleanly and no side product was observed. The results show the excellent catalytic activity of the $\text{Cs}(\text{CTA})_2\text{PW}_{12}\text{O}_{40}$ nanostructure in the preparation of quinoxaline derivatives. The prepared catalyst has the advantages of easy recoverability in comparison with Wells–Dawson heteropoly acid ($\text{H}_6\text{P}_2\text{W}_{18}\text{O}_{62}\cdot 24\text{H}_2\text{O}$) [14] and Keggin-type $\text{H}_4\text{SiW}_{12}\text{O}_{40}$ heteropoly acid [16] catalytic systems and shorter reaction times in comparison with iron exchanged molybdophosphoric acid [15]. On the other hand, solvent-free conditions make it an environmentally friendly and cost-effective process for the preparation of quinoxaline derivatives.

Table 2
Effect of temperature on the reaction times and yields in solvent-free conditions.

Entry	Temperature	Time (h:min)	Yield (%)
1	20	5:00	81
2	40	4:00	80
3	60	2:30	99
4	80	1:15	99
5 ^a	80	24:00	1 >
6 ^b	80	1:15	97

Reaction conditions: benzil (1.0 mmol), *o*-phenylenediamine (1.0 mmol), catalyst (25 mg).

^a The reaction was carried out in the absence of the catalyst.

^b The reaction was carried out with recycled catalyst.

Table 3
Synthesis of quinoxaline derivatives in solvent-free conditions.

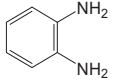
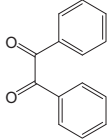
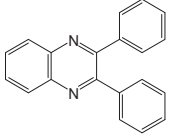
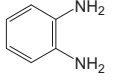
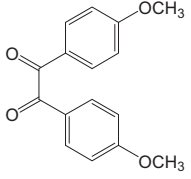
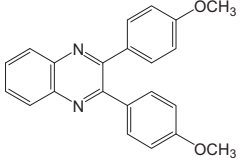
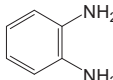
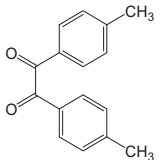
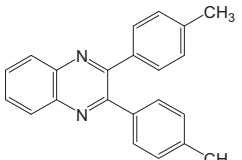
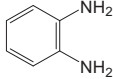
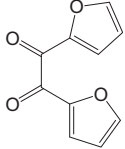
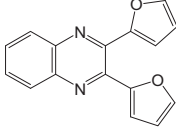
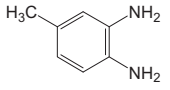
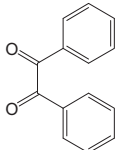
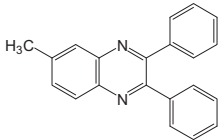
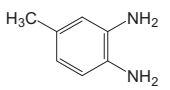
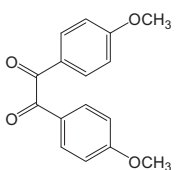
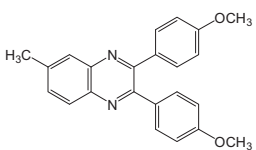
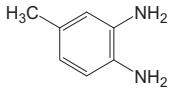
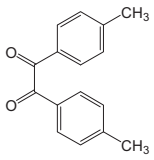
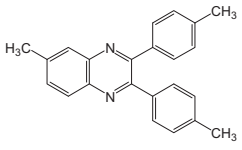
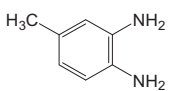
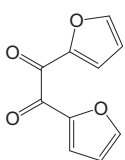
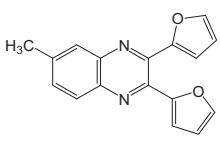
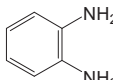
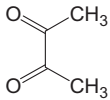
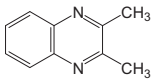
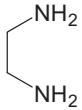
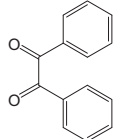
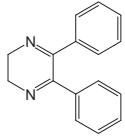
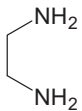
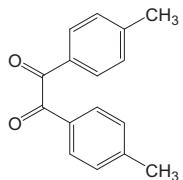
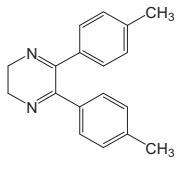
Entry	1,2-Diamine	1,2-Dicarbonyl	Product	Time (h:min)	Yield (%)
1				1:15	99
2				2:15	99
3				00:10	95
4				00:15	99
5				00:30	90
6				1:30	99
7				0:10	99
8				0:10	83
9				0:10	98

Table 3 (Continued)

Entry	1,2-Diamine	1,2-Dicarbonyl	Product	Time (h:min)	Yield (%)
10				0:30	98
11				1:30	62

Reaction conditions: 1,2-diamine (1.0 mmol), 1,2-dicarbonyl (1.0 mmol), catalyst (25 mg), 80 °C.

4. Conclusion

In this paper, we reported the preparation and characterization of a new heteropolytungstate nanostructure by using a microemulsion system. The physicochemical characterizations showed the uniform star-shaped morphology of the product. Our results showed that the proposed method is widely applicable for the preparation of polyoxometalate nanostructures with new morphologies.

On the other hand, we developed a simple, eco-friendly, convenient, and efficient procedure for the synthesis of quinoxalines from the various 1,2-dicarbonyl and 1,2-diamin compounds in the presence of the prepared nanostructure under solvent-free conditions. The procedure offers several advantages, including high yields, short reaction times, cleaner reactions and minimal environmental impact, which make it a useful process for the synthesis of quinoxalines derivatives. The prepared nanostructure behaves as a true heterogeneous catalyst and can be recycled without significant loss of activity with retention of its structure.

References

- P. Kumar, A. Kumar, L.J. Mohan, J.K. Makrandi, *Bull. Korean Chem. Soc.* 31 (2010) 3304.
- M.M. Badran, S. Botros, A.A. El-Gendy, N.A. Abdou, H. El-Assi, A. Salem, *Bull. Pharm. Sci.* 24 (2001) 135.
- A. Kumar, A. Verma, G. Chawla, *Int. J. ChemTech. Res.* 1 (2009) 1177.
- L. Gavara, E. Saugues, G. Alves, E. Debiton, F. Anizon, P. Moreau, *Eur. J. Med. Chem.* 45 (2010) 5520.
- Z. Zhao, D.D. Wisnoski, S.E. Wolkenberg, W.H. Leister, Y. Wang, C.W. Lindsley, *Tetrahedron Lett.* 45 (2004) 4873.
- R.S. Bhosale, S.R. Sarda, S.S. Ardhpure, W.N. Jadhav, S.R. Bhusare, R.P. Pawar, *Tetrahedron Lett.* 46 (2005) 7183.
- L. Bouilly, M. Darabantu, A. Turck, N. Ple, J. Heterocycl. Chem. 42 (2005) 1423.
- S.V. More, M.N.V. Sastry, C.C. Wang, C.F. Yao, *Tetrahedron Lett.* 46 (2005) 6345.
- M. Kidwai, S. Saxena, R. Mohan, *Bull. Kor. Chem. Soc.* 49 (2005) 288.
- T. Huang, R. Wang, L. Shi, X. Lu, *Catal. Commun.* 9 (2008) 1143.
- G. Rezaejade Bardajee, R. Malakooti, F. Jami, Z. Parsaei, H. Atashin, *Catal. Commun.* 27 (2012) 49.
- M. Jafarpour, A. Rezaeifard, M. Danehchin, *Appl. Catal. A* 394 (2011) 48.
- B. Das, K. Venkateswarlu, K. Suneel, A. Majhi, *Tetrahedron Lett.* 48 (2007) 5371.
- M.M. Heravi, K. Bakhtiari, F.F. Bamoharram, M.H. Tehrani, *Monatsh Chem.* 138 (2007) 465.
- K.T. Venkateswara Rao, P.S. Sai Prasad, N. Lingaiah, *J. Mol. Catal. A: Chem.* 312 (2009) 65.
- T.K. Huang, L. Shi, R. Wang, X.Z. Guo, X.X. Lu, *Chin. Chem. Lett.* 20 (2009) 161.
- M.T. Pope, *Heteropoly and Isopoly Oxometalates*, Springer, Berlin, 1983.
- M.T. Pope, A. Muller, *Angew. Chem. Int. Ed. Engl.* 30 (1991) 34.
- J.B. Moffat, *Metal Oxygen Clusters. The Surface and Catalytic properties of heteropoly Oxometalates*, Kluwer, New York, 2001.
- J.F. Keggin, *Proc. R Soc. London Ser. A* 144 (1934) 75.
- M. Misono, *Chem. Commun.* (2001) 1141.
- I.V. Kozhevnikov, *Chem. Rev.* 98 (1998) 171.
- Y. Izumi, K. Urabe, M. Onaka, *Zeolite, Clay and Heteropoly Acid in Organic Reactions*, Kodansha/VCH, Tokyo, 1992.
- M. Misono, I. Ono, G. Koyano, A. Aoshima, *Pure Appl. Chem.* 72 (2000) 1305.
- N. Mizuno, K. Yamaguchi, K. Kamata, *Coord. Chem. Rev.* 249 (2005) 1944.
- I. Mohammadpoor-Baltork, M. Moghadam, S. Tangestaninejad, V. Mirkhani, S.F. Hojati, *Polyhedron* 27 (2008) 750.
- B. Li, Z. Liu, C. Han, W. Ma, S. Zhao, *J. Colloid Interface Sci.* 377 (2012) 334.
- I.V. Kozhevnikov, *Catalysts for Fine Chemical Synthesis, Catalysis by Polyoxometalates, Vol. 2*, Wiley, Chichester, England, 2002.
- T. Nakato, M. Kimura, S. Nakata, T. Okuhara, *Langmuir* 14 (1998) 319.
- E. Rafiee, S. Eavani, F. Khajooei Nejad, M. Joshaghani, *Tetrahedron* 66 (2010) 6858.
- J.A. Dias, E. Caliman, S.C.L. Dias, *Micropor. Mesopor. Mater.* 76 (2004) 221.
- H. Murakami, T. Kozeki, Y. Suzuki, S. Ono, H. Ohtake, N. Sarukura, E. Ishikawa, T. Yamase, *Appl. Phys. Lett.* 79 (2001) 3564.
- L. Cheng, J.A. Cox, *Chem. Mater.* 14 (2002) 6.
- C. Sanchez, G.J.D.A. Solar, F. Ribot, T. Lalot, C.R. Mayer, V. Cabuil, *Chem. Mater.* 13 (2001) 3061.
- T. Ito, K. Inumaru, M. Misono, *Chem. Mater.* 13 (2001) 824.
- R.Y. Wang, D.Z. Jia, L. Zhang, L. Liu, Z.P. Guo, B.Q. Li, J.X. Wang, *Adv. Funct. Mater.* 16 (2006) 687.
- X.H. Zhang, S.Y. Xie, Z.Y. Jiang, L.C. Zhou, Z.X. Xie, R.B. Huang, L.S. Zheng, *Chem. Commun.* (2002) 2032.
- M. Masteri-Farahani, S. Shahbazi, *Inorg. Chem. Commun.* 15 (2012) 297.
- D. Langevin, M.-P. Pileni (Eds.), *Structure and Reactivity in Reverse Micelles*, Elsevier, Amsterdam, 1989.
- V. Pillai, D.O. Shah, in: H. Kunieda, C. Solans (Eds.), *Surfactant Science Series, 66*, Marcel Dekker, New York, 1997.
- V.T. John, B. Simmon, G.L. Mc Pherson, A. Bose, *Curr. Opin. Colloid Interface Sci.* 7 (2002) 288.
- C.R. Deltchev, M. Fournier, R. Franck, R. Thouvenot, *Inorg. Chem.* 22 (1983) 207.
- J.A.F. Gamelas, A.M.V. Cavaleiro, E.D. Gomes, M. Belsley, E. Herdtweck, *Polyhedron* 21 (2002) 2537.